

Optimizing single-photon generation and storage with machine learning

Miao Cai ¹, Yanqing Lu (陆延青)¹, Min Xiao,^{1,2} and Keyu Xia (夏可宇) ^{1,3,*}

¹*College of Engineering and Applied Sciences, National Laboratory of Solid State Microstructures, Collaborative Innovation Center of Advanced Microstructures, and School of Physics, Nanjing University, Nanjing 210093, China*

²*Department of Physics, University of Arkansas, Fayetteville, Arkansas 72701, USA*

³*Jiangsu Key Laboratory of Artificial Functional Materials, and Key Laboratory of Intelligent Optical Sensing and Manipulation, Ministry of Education, Nanjing University, Nanjing 210093, China*



(Received 20 October 2020; revised 11 August 2021; accepted 1 November 2021; published 12 November 2021)

Single photons are at the heart of quantum information processing. The tasks of generating and storing single photons with arbitrary wave-packet shapes are crucial for building quantum networks, but they remain challenging. Here, we present a general machine learning (ML) algorithm with a self-adaptive process to optimize the control of a cavity-atom system for these tasks. This ML algorithm shows high efficiency and fidelity for both generation and storage of single photons. This ML-enhanced single-photon interface may pave the way for building flexible and reliable quantum networks because this ML algorithm can automatically adjust the quantum system according to single-photon wave functions in an “intelligent” way.

DOI: [10.1103/PhysRevA.104.053707](https://doi.org/10.1103/PhysRevA.104.053707)

I. INTRODUCTION

Quantum networks consisting of quantum computation and memory nodes are of great significance for distributed quantum computation and quantum communication [1–9], but they rely crucially on the high-quality generation and memory of single photons. Quantum networks can be realized with cavity quantum electrodynamic (CQED) systems [10–12]. In this CQED scenario, the key functional elements involve photon generation and storage, i.e., mapping the quantum excitation from an atom to a photon in the first CQED system, and then to another atom in the second one.

Generation of single photons has been reported in various quantum systems, such as single trapped atoms [13–15], ions [16,17], single molecules [18,19], quantum dots [20–23], and color centers in diamond [24,25]. When a CQED system is driven by a laser pulse, a single photon with a specific pulse shape can be deterministically generated [26–30]. To accomplish quantum information processing with many photons, on-demand generation of a single photon with an arbitrarily controllable wave packet is highly desired [31].

An outstanding challenge also exists in single-photon storage. Quantum memory has been realized with various methods, such as electromagnetically induced transparency [32–36], a Raman process [37,38], magneto-optical traps [39], or a chiral waveguide QED system [40]. Given the temporal shape of the single-photon input into a CQED system, previous theoretical models for quantum memory allow one to calculate the control laser pulse shape for storing the single photon. However, the existing models mostly focus on specific CQED systems, and they require prerequisite

conditions to derive analytical forms of control laser pulses [27,41–43], therefore they lack generality. It is interesting to develop a general method for storing a single photon with an unknown arbitrary wave packet.

There are intense experimental and theoretical studies on optimizing single-photon generation and storage of CQED systems. Nevertheless, previous analytical and experimental methods can find an optimal control laser pulse only for a specific system configuration in a special parameter regime [27,41–44]. Machine learning (ML), due to its “intelligent” nature, can provide a more general and flexible way to accomplish this challenging task. ML has become a powerful tool for quantum information science and technology [45], including designing, optimizing, and controlling quantum systems [46], recognizing an optical mode [47], characterizing quantum states [48], and reconstructing a quantum channel [49].

In this paper, we propose a general ML algorithm for on-demand generation and efficient memory of a single photon with an arbitrary wave packet in different CQED systems. With this ML algorithm, the CQED systems can generate a single photon with a demanded pulse shape, and they can also store a single photon with an unknown wave function to a single atom with varied energy-level structures.

This paper is organized as follows: In Sec. II, we first introduce the scheme of single-photon generation and storage in a typical Λ -type CQED system with one excited state. Then, we take into account the full energy-level structure of the atom to extend our CQED system to include multiexcited states. Using these systems, we propose in Sec. III a ML algorithm to obtain the control laser pulse that can realize on-demand generation and efficient memory for a single photon with an arbitrary wave packet. In the end, we apply in Sec. IV our ML algorithm to previous CQED systems, and we show that both systems can generate and store a single photon with an

*keyu.xia@nju.edu.cn

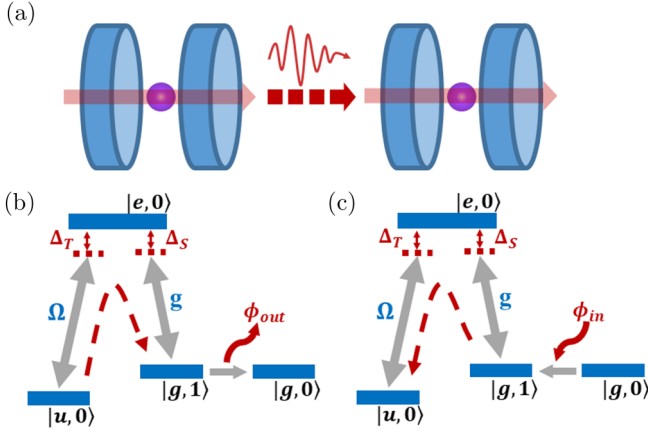


FIG. 1. Schematic of single-photon generation and storage for a CQED-based quantum network. (a) The CQED-based quantum network, showing the quantum information transfers from an atom in one CQED node to an atom in another CQED node via single photons. (b) Single-photon generation scheme with a Λ -type three-level atom coupling to the cavity mode and driven by a control laser pulse Ω . The atom has two ground states $|u\rangle$ and $|g\rangle$ and an optical excited state $|e\rangle$. The states $|0\rangle$ and $|1\rangle$, respectively, represent the zero- and one-photon states of the cavity mode. ϕ_{out} is the outgoing wave function of the single photon emitted to the quantum channel. (c) Schematic for single-photon storage with a three-level atom in a cavity and driven by a control laser pulse. ϕ_{in} is the incoming wave function of the input single photon to be stored. The control laser pulses and the cavity mode are detuning from the atomic transitions by Δ_T and Δ_S , respectively.

arbitrary wave packet. Section V contains a discussion of our work and our conclusions.

II. SYSTEM AND MODEL

Among CQED systems, atoms with three-level structures are widely used to achieve single-photon emission and absorption by coupling to optical cavities. Many efforts have been made to theoretically obtain an optimal control field for on-demand single-photon generation and storage in a typical Λ -type CQED system [41,43,44]. However, schemes using CQED systems in which atoms have more complex energy-level structures have rarely been studied [41]. Below, we first introduce a single-photon generation and storage scheme in a Λ -type CQED system with an atom having only one excited state. Then, we consider a more complex case in which the atom has three excited states (3ES) in the CQED system. Using this 3ES-CQED system, we elaborate on its single-photon generation and storage process.

A. Λ -type CQED system with one excited state

The schematic of single-photon generation and storage setup in the CQED systems using a Λ -type atom with only one excited state (1ES) is depicted in Fig. 1(a). It schematically shows quantum information transfers from one CQED node to another via single photons. The quantum information stored in the atom in the first CQED node is first mapped into a single photon through the photon generation step, and then

transferred into the second atom when the single photon is stored in the second CQED node.

The CQED nodes for single-photon generation and storage have the same configuration, namely a Λ -type atom with one excited state coupling to a cavity, but they can have different parameter values, as shown in Figs. 1(b) and 1(c), respectively. In each CQED node, the cavity mode couples to a Λ -type atom with the ground states $|u\rangle$ and $|g\rangle$, and the excited state $|e\rangle$. The states $|0\rangle$ and $|1\rangle$ denote the zero- and one-photon cavity field, respectively. The cavity mode couples at a strength g to the transition between $|e\rangle$ and $|g\rangle$ with a detuning Δ_S . A classic laser field Ω (named as the control laser pulse) drives the transition between $|e\rangle$ and $|u\rangle$ and is detuned by Δ_T . In the associated configuration of the atom and the cavity mode, a Raman transition forms between $|u, 0\rangle$ and $|g, 1\rangle$. Although the generation and storage of single photons share the same configuration, their operations are different.

For single-photon generation shown in Fig. 1(b), the CQED system is initially prepared in the dressed state $|u, 0\rangle$. Driven by $\Omega(t)$, the quantum excitation is first transferred to the cavity mode $|g, 1\rangle$ via the Raman transition. Then, the photon is emitted into the output channel through one of two mirrors forming the cavity, generating a single-photon wave packet in the state $|g, 0\rangle$ denoted as ϕ_{out} and leaving the system in the state $|g, 0\rangle$. Applying the two-photon resonance condition, i.e., $\Delta_S = \Delta_T = \Delta$, and taking the set of states $\{|u, 0\rangle, |e, 0\rangle, |g, 1\rangle\}$ as the basis, the interaction Hamiltonian in the interaction pictures can be written as

$$H = -\frac{\hbar}{2} \begin{pmatrix} 0 & \Omega & 0 \\ \Omega^* & \Delta_S + \Delta_T & 2g \\ 0 & 2g^* & 0 \end{pmatrix}. \quad (1)$$

The single-photon generation process can be determined by solving the master equation

$$\dot{\rho} = -\frac{i}{\hbar}[H, \rho] - \Gamma\rho, \quad (2)$$

where ρ is the density matrix, and Γ is a linear superoperator describing all relaxation. The elements of $\Gamma\rho$ can be expressed in terms of the relaxation rate γ_i of each state. Here, the relaxation processes of states $|e, 0\rangle$ and $|g, 1\rangle$ are denoted as $\gamma_2 = \gamma$ and $\gamma_3 = 2\kappa$, respectively. γ_1 is zero because there is no relaxation from $|u, 0\rangle$, which is the atomic ground and cavity vacuum state. Einstein coefficients A_{ki} represent spontaneous transitions between the basis states [26],

$$[\Gamma\rho]_{ij} = \frac{1}{2}(\gamma_i + \gamma_j)\rho_{ij} - \delta_{ij} \sum_k \rho_{kk} A_{ki}, \quad (3)$$

with $i, j = 1, 2, 3$. For convenience, we use subscripts $\{1, 2, 3\}$ to relate parameters and variables to the basis $\{|u, 0\rangle, |e, 0\rangle, |g, 1\rangle\}$ in the following investigation. The first term on the right-hand side of Eq. (3) only includes the damping or losses of $\rho_{i,j}$. The second term describes the incoherent population shift into basis states. The two ground states $|u, 0\rangle$ and $|g, 0\rangle$ are populated at a nearly equal rate by the spontaneous emission from $|e, 0\rangle$. In this case, the only nonzero Einstein coefficient is $A_{21} = \frac{1}{2}\gamma$. The decay in another channel $|e, 0\rangle \rightarrow |g, 0\rangle$ is already included in γ . Note that no decay happens in the process $|e, 0\rangle \rightarrow |g, 1\rangle$ because this process is a coherent transition caused by the coupling between the atom and the cavity, where excitation remains unchanged. The wave

packet of the generated single photon $\phi_{\text{out}}(t)$ is proportional to the population ρ_{33} , determined as $\phi_{\text{out}}(t) = 2\kappa\rho_{33}(t)$. This wave function $\phi_{\text{out}}(t)$ can be calculated with Eq. (2) and is controlled by the control laser pulse $\Omega(t)$.

As shown in Fig. 1(c), we consider the reverse process of the single-photon generation for storage. Under the two-photon resonance condition that $\Delta_T = \Delta_S = 0$, we can characterize the storage process of the input single photon ϕ_{in} by solving the probability amplitude equation [27]

$$\begin{pmatrix} \dot{c}_1 \\ \dot{c}_2 \\ \dot{c}_3 \\ \dot{\phi}_{\text{out}} \end{pmatrix} = \begin{pmatrix} 0 & -i\frac{\Omega^*}{2} & 0 & 0 \\ -i\frac{\Omega}{2} & -\gamma & -ig & 0 \\ 0 & -ig^* & -\kappa & \sqrt{2\kappa} \\ 0 & 0 & \sqrt{2\kappa} & -r \end{pmatrix} \begin{pmatrix} c_1 \\ c_2 \\ c_3 \\ \phi_{\text{in}} \end{pmatrix}, \quad (4)$$

where c_i is the probability amplitude of each state. ϕ_{out} is the leakage of the single photon to be stored. Ideally, $\phi_{\text{out}} = 0$ and $|c_1|^2 = 1$. The key point is to find a proper control laser pulse $\Omega(t)$ to ensure that $|c_1|^2$ reaches as close to unity as possible.

If the control laser pulse $\Omega(t)$ and all control parameters in the generation process are known, the emitted single photon has a well-defined wave function. Therefore, a simple way to optimize the single-photon storage is to apply a time-reversed control laser pulse $\Omega(-t)$ in the storage system identical to the generation one [42]. Previous studies have also obtained analytical solutions of an optimal control laser pulse for storage in the 1ES-CQED system [43,44]. However, the validity of the analytical solution is limited by theoretical assumptions and a specific system structure, thus there is a lack of generality. Therefore, it is highly desirable to build quantum networks in order to develop a general method to store a single photon with an arbitrary wave function in different CQED systems.

B. Λ -type CQED system with three excited states

In the aforementioned 1ES-CQED system, the Λ -type atom only includes one excited state. It is the simplest energy level structure of a Λ -type atom. Therefore, to show the generality and flexibility of our ML-based scheme, we extend our investigation to the 3ES-CQED system, which is a complex atomic configuration with three excited states.

As depicted in Fig. 2, a single Λ -type atom with three excited states couples to an optical cavity. The control laser pulse $\Omega(t)$ impinges from the side of the cavity, coupling the ground state of the atom with its excited states. Combining the cavity-atom coupling, the system is able to serve as a single-photon emitter and a receiver. The cavity is formed out of two asymmetric mirrors: one is assumed to be highly reflective, while the other has a relatively low reflectivity. We denote the decay rates via two mirrors of the cavity as κ_c and κ_l , respectively.

The details of the single-photon generation and storage process in this CQED system are shown in Fig. 2(b). The cavity field couples the ground state $|g\rangle$ to the excited states $|e_1\rangle$ and $|e_2\rangle$ with coupling strength g_i with $i \in \{1, 2\}$, where the subscripts indicate different excited states. The control laser pulse addresses the transition process $|u\rangle \rightarrow |e_i\rangle$ with Ω_i ($i \in \{1, 2, 3\}$), respectively. Following the model in Ref. [41], we define the associated cavity coupling strength, g_i , and

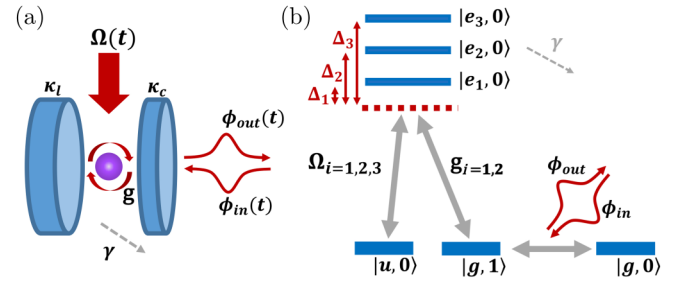


FIG. 2. Single-photon generation and storage model of the CQED system where the atom has three excited states. (a) A single atom trapped in an optical cavity. The control laser pulse $\Omega(t)$ couples the ground state of the atom to its excited states. The constant g represents the coupling strength between the atom and the cavity, and the atomic polarization decay (gray dashed arrow) rate is denoted as γ . (b) We use a single atom with three excited states. The atom has two ground states, $|u\rangle$ and $|g\rangle$, and three optical excited states $|e_i\rangle$ ($i \in \{1, 2, 3\}$). The zero- and one-photon states of the cavity mode are denoted as $|0\rangle$ and $|1\rangle$. ϕ_{out} and ϕ_{in} represent the temporal wave function of the emitted and injected single photon, respectively. The control laser pulses and the cavity mode are detuned from the atomic transitions by Δ_i for each excited state.

control laser pulse, Ω_i , as

$$g_i = c_{gi}g, \quad \Omega_i = c_{ui}\Omega, \quad (5)$$

where c_{gi} (c_{ui}) are the Clebsch-Gordan coefficients for the transition between the ground state $|g\rangle$ ($|u\rangle$) and the excited states $|e_i\rangle$. For convenience, we take the Clebsch-Gordan coefficients as unity in this work. To selectively driving the excited states in our configuration, we need control laser beams with frequency splittings from several hundred megahertz to a few gigahertz. Such narrow separated laser beams can be generated with an acoustic-optics modulator (AOM) [50–53].

As shown in Fig. 2(b), the detunings of each excited state Δ_i with $i \in \{1, 2, 3\}$ are the same for both the cavity field and the control light field, thus the Λ scheme is in two-photon resonance. With the combination of two fields, the atomic population is driven from the state $|u, 0\rangle$ to $|g, 0\rangle$ in single-photon generation and vice versa for storage. In addition, we refer to the temporal wave function of the output single photon as $\phi_{\text{out}}(t)$ in the generation process (or leakage in the storage scheme), whereas $\phi_{\text{in}}(t)$ denotes the wave function of the input single photon in the single-photon storage process, which continues to be zero in the generation process. Thus, we can describe both single-photon generation and the storage process in this CQED system by solving the following probability amplitude equations [41]:

$$\begin{aligned} \dot{c}_u &= i\frac{1}{2}\Omega_1^*c_{e_1} + i\frac{1}{2}\Omega_2^*c_{e_2} + i\frac{1}{2}\Omega_3^*c_{e_3}, \\ \dot{c}_{e_1} &= i\frac{1}{2}\Omega_1c_u - (\gamma + i\Delta_1)c_{e_1} + ig_1c_g, \\ \dot{c}_{e_2} &= i\frac{1}{2}\Omega_2c_u - (\gamma + i\Delta_2)c_{e_2} + ig_2c_g, \\ \dot{c}_{e_3} &= i\frac{1}{2}\Omega_3c_u - (\gamma + i\Delta_3)c_{e_3}, \\ \dot{c}_g &= ig_1c_{e_1} + ig_2c_{e_2} - \kappa c_g + \sqrt{2\eta_{\text{esc}}\kappa}\phi_{\text{in}}, \\ \dot{\phi}_{\text{out}} &= \sqrt{2\eta_{\text{esc}}\kappa}c_g - \phi_{\text{in}}, \end{aligned} \quad (6)$$

where c_i is the probability amplitude of each state, γ is the atomic polarization decay rate, and $\kappa = \kappa_c + \kappa_l$ is the cavity field decay rate. $\eta_{\text{esc}} = \kappa_c/\kappa$ is the escape efficiency, which represents the ratio of the probability of cavity field escape through the output field to the total escape probability (including the output field and the losses channel).

Compared with the CQED system described in Sec. II A, the CQED system in this subsection has a more complicated energy-level structure. Therefore, it is more difficult to analytically obtain the optimal control laser pulse for single-photon generation with a demanded wave function without assumption. For a single-photon storage scheme, it is even more challenging to obtain an analytical function of a control laser pulse considering the phase of the input single photon. Since the energy-level structure of the atom may differ from the ideal situation in experiment, it is key for building a robust CQED-based quantum network to develop a method that can realize on-demand single-photon generation and efficient storage and does not depend on specific atomic structures. In this work, we present a ML algorithm to achieve this.

III. ALGORITHM

Many efforts have been made to control single-photon emission and to find a proper control laser pulse for optimizing single-photon storage [41,42,54]. These methods typically can either solve the photonic wave function or store a single photon in an atomic state when the control laser pulse in generation [11] or the wave function [41] is already known in a simple 1ES-CQED system. Here, we present a ML algorithm independent of specific system configurations to obtain the control laser pulse Ω for generating and storing a single photon with an arbitrary wave packet.

A. Reinforcement learning theory

Our ML algorithm is developed from the basic idea of the reinforcement learning (RL) theory [55]. RL is a ML approach for solving the reward-based problem. Generally, a RL system consists of three parts: a *policy*, a *reward signal*, and a *value function*. The policy defines the learning agent's actions over time. Therefore, a policy Π can be expressed as an action sequence $\Pi \equiv \{\Pi_{t_1}, \Pi_{t_2}, \dots\}$ over discrete time $\{t_i\}$. The reward signal, denoted as R_{t_i} , is the benefit from an action at a given time t_i . Thus, the reward signal can be considered as a function of the action: $R_{t_i} = f_{\text{reward}}(\Pi_{t_i})$. While the reward signal indicates the benefit in a temporary sense, the value function V makes an overall evaluation of the actions from the beginning time t_1 to the present time t_i : $V = f_{\text{value}}(\{\Pi_{t_1}, \Pi_{t_2}, \dots, \Pi_{t_i}\})$.

The ultimate goal of RL is to find the optimal policy to maximize the value function. A general method to achieve the goal is the policy iteration algorithm, which proceeds as shown in the following pseudocode. Here we assume that the optimization of each reward signal function is equal to the optimization of the overall value function. By choosing an appropriate reward signal function and value function, one can always adopt this assumption.

Algorithm 1 Finding the optimal policy Π to maximize the value function V . $f_{\text{reward}}(\Pi_{t_i})$ denotes the reward signal function of one step policy Π_{t_i} at a given time t_i . $f_{\text{renew}}(\Pi_{t_i})$ denotes the renew function of each step policy, and it can vary according to particular problems.

Input: N : number of time steps; K : maximum number of iterations;
Output: the optimal policy Π .

- 1: initialize the policy Π
- 2: **for** i in $\{1, 2, \dots, N\}$ **do**
- 3: **for** j in $\{1, 2, \dots, K\}$ **do**
- 4: **if** $\Pi_{t_i} = \arg \max_{\Pi_{t_i}} f_{\text{reward}}(\Pi_{t_i})$
- 5: **break**
- 6: **else**
- 7: $\Pi_{t_i} \leftarrow f_{\text{renew}}(\Pi_{t_i})$
- 8: **end if**
- 9: **end for**
- 10: **end for**

B. ML algorithm for a CQED system

Without loss of generality, we use the 1ES-CQED system shown in Sec. II A to explain the idea of our ML algorithm in detail. In this case, the policy indicates the control laser pulse's value at a given time. The reward signal corresponds to the error between the output single-photon wave function and the target of our quantum system in each time segment in our ML algorithm. In our system and ML algorithm, the value function is the fidelity between the generated single-photon wave function and the target for the single-photon generation, and the efficiency of the storage. Throughout the investigation below, we replace the phrases “policy,” “reward signal,” and “value function” with “control laser pulse,” “error,” and “fidelity” or “efficiency” for a more physical purpose.

As preparation for implementing the algorithm, the training datasets $\{I_j\}$ and $\{O_j\}$ are generated from the control laser pulse $\Omega(t)$ and the target single-photon wave function $\phi_{\text{out}}^{(T)}(t)$, as schematically depicted in Fig. 3(a). To do so, we divide $\Omega(t)$ and $\phi_{\text{out}}^{(T)}(t)$ into N time segments, each with a time

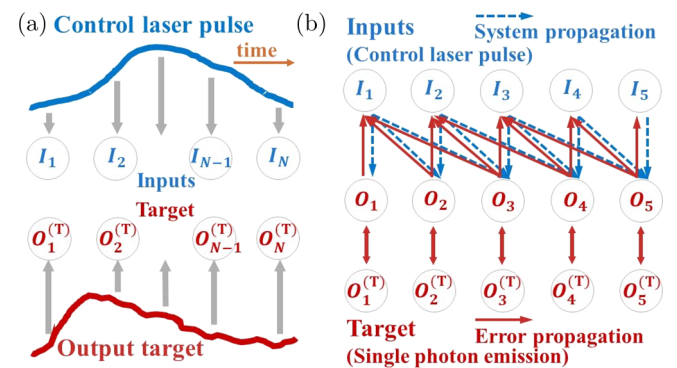


FIG. 3. Discretization of the ML algorithm for single-photon generation. (a) Control laser and target single-photon pulses are discretized as the input and target datasets for training, respectively. (b) Schematic showing the key routine for training under an extended Markov assumption. The inputs $\{I_j\}$ [$\Omega(t)$ in the physical model] to be trained generate the outputs $\{O_j\}$ [$\phi_{\text{out}}(t)$] by solving Eq. (2).

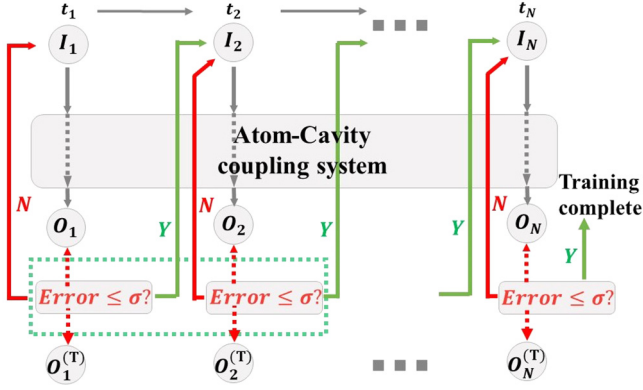


FIG. 4. Detailed ML algorithm of Fig. 2(b). The input dataset (discrete control laser pulse) iteratively adjusts itself until the error (feedback in training) between the estimated output and the target value becomes small enough.

interval of Δt . We use the average values, $\int_{t_{j-1}}^{t_j} \Omega(t)/\Delta t dt$ and $\int_{t_{j-1}}^{t_j} \phi_{\text{out}}(t)/\Delta t dt$ with $t_j = (j - 1/2)\Delta t$ ($j \in \{1, 2, \dots, N\}$), of the pulses $\Omega(t)$ and $\phi_{\text{out}}(t)$ in the j th time segment as a good approximation to replace the discrete values I_j and O_j .

Then, to maximize the fidelity, adjustment is iteratively implemented on the control laser pulse Ω until the error is small enough, which means that the difference between the output single-photon wave function and the target is negligible. The most crucial point in this process is the training rules in each iteration, which are designed based on an intuitive but effective hypothesis: the value of ϕ_{out} at time t is related to the integral of $\Omega(t)$ from time t_0 to t , mathematically being

$$\phi_{\text{out}}(t) \propto \int_{t_0}^t k(t')\Omega(t')dt', \quad (7)$$

where the coefficient $k(t) \geq 0$ is time-dependent and needs to be adjusted during training.

To perform the ML algorithm, the control laser pulse and target single-photon wave function are transferred into the discrete datasets $\{I_i\}$ and $\{O_i^{(T)}\}$, as shown in Fig. 3(b). The blue dashed arrows represent the positive correlation, i.e., $k(t) \geq 0$, between the control laser pulse as the input and the single-photon pulse as the output. To improve the training efficiency of the ML algorithm, we take an extended Markov assumption [56] so that each output ML node's value is only related to a few previously input ML nodes. By applying this assumption and discretizing the outgoing single-photon and control laser pulses, the relation Eq. (7) becomes $\phi_{\text{out}}(t) \approx k(t) \sum_{j=N-m}^N \Omega(t_j)\Delta t$, where m is the number of previous ML nodes to be considered. Note that the choice of m is independent of the CQED system parameters, and it has an influence on the amount of calculation in each training step. This assumption can greatly speed up our algorithm while maintaining sufficient accuracy.

The full training process of the ML algorithm is schematically depicted in Fig. 4. First, we arbitrarily choose a control laser pulse as the initial input dataset $\{I_i\}$, and we generate the dataset $\{O_i^{(T)}\}$ for the target single-photon wave function. Here, we set the initial input zero in the first training step. Then, we use the interpolation method to convert the discrete input dataset into a continuous function $\Omega(t)$. After

that, we substitute $\Omega(t)$ into Eq. (2) and numerically calculate the single-photon wave function $\phi_{\text{out}}(t)$. Then, $\phi_{\text{out}}(t)$ is discretized as the output dataset $\{O_i\}$. In the fourth step, we calculate the error set from the target value $\{O_i^{(T)}\}$ and the output $\{O_i\}$ in the i th time step, denoted as e_i . For the i th time step in the j th iteration in training, the ML rule can be written as [57]

$$I_i^{j+1} \leftarrow I_i^j + \eta e_i^j, \quad (8)$$

where $\eta \in (0, 1]$ is the learning rate. For each training step, the training process continues until the error is negligible or the number of iterations exceeds a preset value in order to avoid an endless loop. This process is performed step by step. We apply the extended Markov assumption to the input-to-output process and error propagation in Fig. 3(b). When training the input I_j , we keep updating the values of I_s with $(j - m) \leq s \leq j$. In doing so, the error between the output and the target datasets propagates to the previous m input ML nodes, as shown by red arrows in Fig. 3(b). Finally, when the training of all steps is completed, the wanted control laser pulse is obtained. Then, using this trained laser pulse to drive the cavity-atom system, we can create the target single-photon wave function with a nearly unitary fidelity. To clearly explain our ML algorithm, we provide the pseudocode of the complete training process in the following.

Algorithm 2 Training the control laser pulse for single-photon generation in the IES-CQED system. The operation function $f_{\text{discrete}}(T, F(t), N)$ discretizes a time-dependent function $F(t)$ within the time range T into a discrete dataset $\{F'\}$ containing N data points. The function $f_{\text{interp}}(\{F'\}, \{T'\})$ performs the interpolation method to transform the discrete dataset $\{F'\}$ into a continuous time-dependent function $F(t)$ according to the discrete time set $\{T'\}$ order. The function $f_{\text{phys}}(T, \Omega(t), \gamma, \kappa, g)$ gives the numerical solution for the system output when $\{T, \Omega(t), \gamma, \kappa, g\}$ are given.

Input: $\phi_{\text{out}}^{(T)}(t)$: target single-photon wave function; N : number of time segments; K : number of maximum iterations; T : time range; e_{min} : acceptable minimum error; $\{\gamma, \kappa, g\}$: IES-CQED system parameters; η : learning rate.

Output: fully trained control laser pulse $\Omega(t)$.

initialize $\Omega(t) = 0$, $t \in [0, T]$.

2: $\{T'_i\} \leftarrow f_{\text{discrete}}(T, T, N)$, $i = \{1, 2, \dots, N\}$.

$\{I_i\} \leftarrow f_{\text{discrete}}(T, \Omega(t), N)$, $i = \{1, 2, \dots, N\}$.

4: $\{O_i^{(T)}\} \leftarrow f_{\text{discrete}}(T, \phi_{\text{out}}^{(T)}(t), N)$, $i = \{1, 2, \dots, N\}$.

for i in $\{1, 2, \dots, N\}$ **do**

6: **for** j in $\{1, 2, \dots, K\}$ **do**

$\Omega(t) \leftarrow f_{\text{interp}}(\{I_i\}, \{T'_i\})$

8: $\phi_{\text{out}}(t) \leftarrow f_{\text{phys}}(T, \Omega(t), \gamma, \kappa, g)$

$\{O_i\} \leftarrow f_{\text{discrete}}(T, \phi_{\text{out}}(t), N)$

10: $e_i^j = O_i^{(T)} - O_i$

$I_i \leftarrow I_i + \eta e_i^j$

12: **if** $e_i^j \leq e_{\text{min}}$

break

14: **end for**

end for

The single-photon storage is different from the photon generation. The target output (the leakage ϕ_{out}) is zero if the input single photon is fully transferred to an atomic excitation as

expected. Given an input single-photon wave function ϕ_{in} and the control laser pulse Ω , we can calculate the output ϕ_{out} with Eq. (4). For storage purposes, we consider the control laser pulse as the training object, and we set the target output ϕ_{out} to zero during the training process, as shown in Fig. 4. Besides, if the phase term of the input single photon is considered, $\Omega(t)$ needs to be treated as a complex function. In this case, we apply our ML algorithm to both the real and imaginary parts of $\Omega(t)$ simultaneously. The rest of the ML algorithm is the same as the generation scheme. Note that the single-photon wave function is given only for demonstrating our ML algorithm; it is not needed in practical operation.

IV. RESULT

Contrary to the analytical method, our ML algorithm is suitable for both single-photon generation and the storage process, and it is independent of the specific configuration of the CQED system. Below, we show that our ML algorithm can find the optimal control laser pulses for single-photon generation and storage in both 1ES-CQED and 3ES-CQED systems. The hyperparameters we used in the ML algorithm to obtain the results are presented in Appendix A, together with the resource and the time consumption information of our ML algorithm.

A. 1ES-CQED system

We first evaluate the performance of the ML algorithm for single-photon generation in the CQED system demonstrated in Sec. II A. For an arbitrary wave function of a single photon, we can find a control laser pulse with this algorithm. To show the performance of the ML algorithm, we take four different single-photon wave functions: sinusoidal-, Gaussian-, square-, and triangular-shaped. As for system parameters, we refer to the commonly used parameter ranges in the existing works [26,41]. Therefore, we choose the same system with parameters for all four cases: $\{\kappa = 2\pi \times 0.75 \text{ MHz}, \gamma = 2\pi \times 3 \text{ MHz}, g = 2\pi \times 9 \text{ MHz}, \Delta = 2\pi \times -20 \text{ MHz}\}$.

The trained control laser pulse, the generated single-photon wave function, and the corresponding fidelity are shown in Fig. 5. It can be seen from Fig. 5(a) that the generated single-photon pulse becomes closer and closer to the target pulse for four different pulses as the training is going on (from top to bottom). In principle, our training method works well no matter what shape the target single-photon pulse has. The fidelity, defined as [58], of the output single-photon wave function after N -step training is shown in Fig. 5(b). The ‘‘training step n ’’ represents the accumulating time step to which the training progresses. Each subfigure in Fig. 5(a) corresponds to a fidelity value at a specific training step in Fig. 5(b). The fidelity increases as the training process goes on. It finally approaches unity for four different target single-photon wave functions when the full control laser pulse is trained out: 99.64% for the sinusoidal shape, 96.09% for the Gaussian shape, 98.44% for the square shape, and 99.87% for the triangular shape. The fidelity can be further improved by increasing the number of training segments and choosing an appropriate learning rate η .

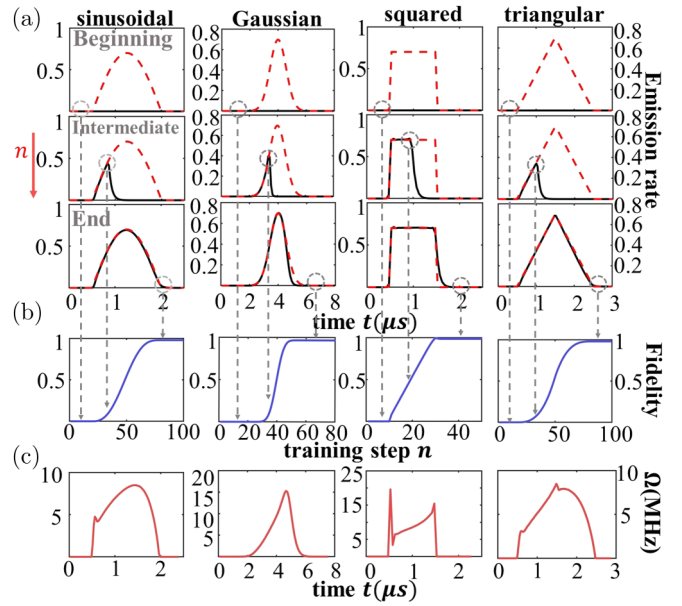


FIG. 5. Single-photon generation using a 1ES-CQED system with parameters $\kappa = 2\pi \times 0.75 \text{ MHz}$, $\gamma = 2\pi \times 3 \text{ MHz}$, $g = 2\pi \times 9 \text{ MHz}$, and $\Delta = 2\pi \times -20 \text{ MHz}$. (a) The target (dashed red curves) and output (black curves) single-photon wave functions during training. Plots in the top row show the wave functions in the beginning, the middle row for the intermediate results after parts of the control laser pulse are trained, and the bottom row for the final generated single-photon pulses after the training is completed. (b) Fidelity as the training steps increase. Gray dashed arrows link the fidelity at a specific training step to the output single-photon wave functions during the training process. (c) Fully trained control laser pulses.

After the training process is completed, we obtain the full control laser pulse for generating the corresponding target single-photon pulses with demanded shapes shown in Fig. 5(c). Note that the control laser pulses $\Omega(t)$ for the square- and triangular-shaped single-photon pulses are derivative discontinuous, because the target single-photon wave functions are derivative-discontinuous. Obviously, $\Omega(t)$ has no analytic form in the four cases, and it is difficult to find using the methods in [42]. However, our ML algorithm can find the proper $\Omega(t)$ for generating the target single-photon pulses with high fidelity, regardless of its derivation continuity. The fast temporal modulation of the obtained control laser pulse relies on the control technique shaping laser pulses in less than $0.1 \mu\text{s}$. This technique is experimentally available [59–61]. In addition, we can adjust the changing rate of the obtained control laser pulse with the time segment value of the discrete input dataset depicted in Fig. 4.

Below we justify the robustness and generality of our ML algorithm with a precision-limited CQED system of which the values of the parameters vary within a small range or they are imprecisely premeasured. First, we assume a ‘‘perfect-training’’ 1ES-CQED system and apply our ML algorithm in it to obtain the fully trained control laser pulse for a target wave function. By ‘‘perfect-training,’’ we mean that the system parameters are precisely known and thus our ML algorithm can perfectly optimize the control fields. Then, we consider the variation of parameters in the system. We apply the

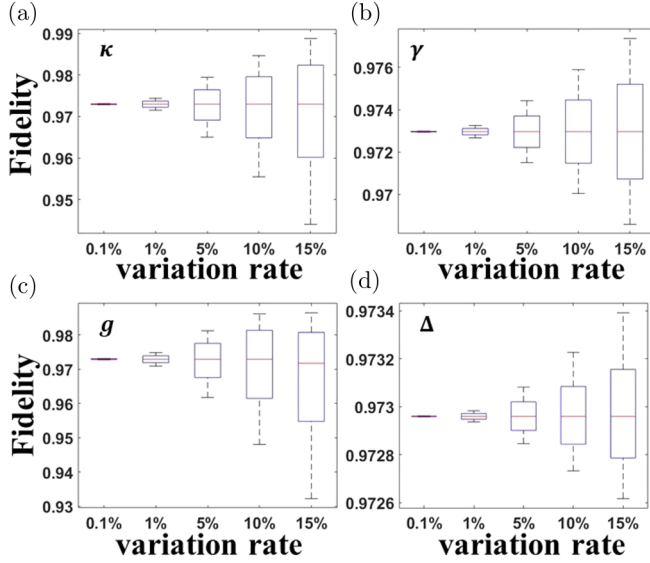


FIG. 6. Fidelity as the CQED system parameters change in different variation ranges. Each panel corresponds to a specific parameter as depicted in the upper left corner of each diagram. The horizontal axis represents the variation range of the corresponding parameter varying from the value used for training. The box plot in each panel describes the fidelity distribution of each variation rate.

obtained control laser pulse to this deviate system and calculate the fidelity between the output of the imperfect system and the target wave function trained in the perfect-training system.

Now, we take the 1ES-CQED system shown in Sec. II A with parameters $\{\kappa = 2\pi \times 0.75 \text{ MHz}, \gamma = 2\pi \times 3 \text{ MHz}, g = 2\pi \times 9 \text{ MHz}, \Delta = 2\pi \times -20 \text{ MHz}\}$ for our justification. The corresponding target wave function is Gaussian-shaped. The obtained fidelity for the deviate system with different variation in parameters is shown in Fig. 6. The horizontal axis indicates the variation range of the system parameters (e.g., “15%” represents the variation range of $\pm 15\%$ with respect to the parameter value in the perfect-training system). The fidelity is calculated with parameters uniformly distributed in the corresponding variation range. As we can see from Fig. 6, the fidelity maintains above 93% even when the parameter varies up to 15%. The results clearly prove the strong robustness of our ML algorithm against parameter variation.

We can also apply our ML algorithm to find specific control laser pulses to store single photons with arbitrary wave functions in the same CQED system. We take three different single-photon wave functions: sine-square-, square-, and triangular-shaped. For all three cases, the parameters of the system are identical: $\{\kappa = 2\pi \times 3 \text{ MHz}, \gamma = 2\pi \times 3 \text{ MHz}, g = 2\pi \times 15 \text{ MHz}\}$. We take parameter values different from the generation value to show the robustness of our ML method.

The photon leakage during training, the storage efficiency, and the trained control laser pulse are shown in Fig. 7. Clearly, the leakage gradually approaches zero as the training process is going on for all three different input pulses. The efficiency is slightly smaller than the ideal one due to the atomic decay [41]. Note that the control pulse values at

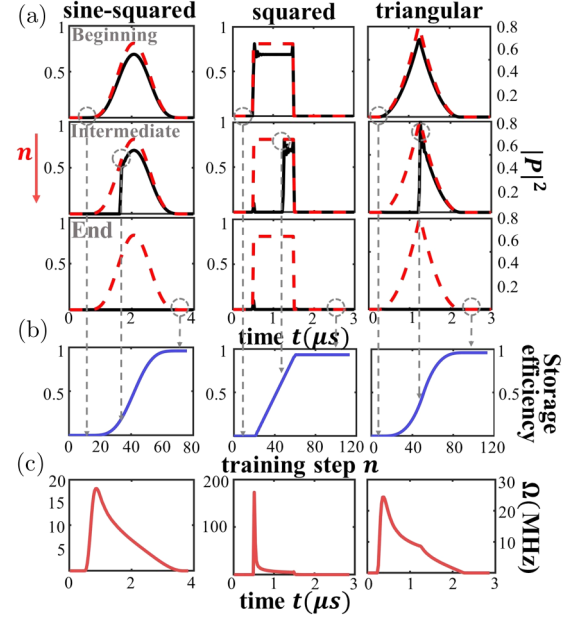


FIG. 7. Single-photon storage using a 1ES-CQED system with parameters $\{\kappa = 2\pi \times 3 \text{ MHz}, \gamma = 2\pi \times 3 \text{ MHz}, g = 2\pi \times 15 \text{ MHz}\}$. (a) The input single-photon wave function (dashed red curves) and the leakage (black curves) during the training process. Each column of panels is arranged in the order of training times from top to bottom. (b) Storage efficiency as the training steps increase. (c) Trained control laser pulses.

neighboring training ML nodes may differ greatly, leading to fast but small oscillation in the leakage; see the middle row of Fig. 5(a). After training is completed, the oscillation vanishes.

In an ideal situation, the input single photon can be perfectly stored in the ground state $|u, 0\rangle$. We refer to the population in the state $|u, 0\rangle$ as the storage efficiency. The ideal single-photon storage efficiency is given by $\eta_c = 2C/(2C + 1)$, where C is the cooperativity defined as $C = g^2/2\kappa\gamma$ [41]. It is 96.15%. It can be seen from Fig. 7(b) that the storage efficiency gradually approaches the ideal efficiency for all three cases: 95.91% for the sine-square shape, 93.29% for the square shape, and 95.87% for the triangular shape. The trained control laser pulses are shown in Fig. 7(c).

B. 3ES-CQED system

To further prove the generality and robustness of our ML algorithm, we apply it to obtain the optimal control laser pulse for single-photon generation and storage in a more complicated CQED system shown in Sec. II B.

For single-photon generation, we take a Gaussian-shaped wave function as the target. To compare the performance of our algorithm applied to the 1ES- and 3ES-CQED systems, we set the 3ES-CQED system with the same system parameters as in the 1ES-CQED one: $\{\kappa_c = 2\pi \times 0.75 \text{ MHz}, \kappa_l = 0, \gamma = 2\pi \times 3 \text{ MHz}, g = 2\pi \times 9 \text{ MHz}, \Delta_1 = 72.2 \text{ MHz}, \Delta_2 = 229.1 \text{ MHz}, \Delta_3 = 495.8 \text{ MHz}\}$. Here, we take $\kappa_l = 0$ so that the escape efficiency η_{esc} of the cavity is unity. In addition, we choose the detunings Δ_i as in the previous experiment work [41] to validate the performance of our algorithm in a

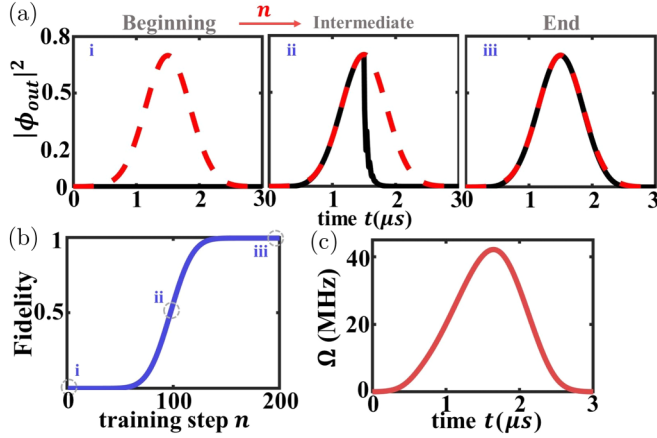


FIG. 8. Single-photon generation using a 3ES-CQED system with parameters $\kappa_c = 2\pi \times 0.75$ MHz, $\kappa_l = 0$, $\gamma = 2\pi \times 3$ MHz, $g = 2\pi \times 9$ MHz, $\Delta_1 = 72.2$ MHz, $\Delta_2 = 229.1$ MHz, and $\Delta_3 = 495.8$ MHz. (a) The target (dashed red curves) and output (black curves) single-photon wave functions during training. (b) Fidelity increases as the training steps increase. The output wave functions (black curves) in (a) correspond to the training steps labeled as (i), (ii), and (iii) in (b). (c) Completely trained control laser pulse.

real system. The emitted photon output, the associated fidelity, and the trained control laser pulse are shown in Fig. 8. Obviously, the generated single-photon pulse gradually reaches the target pulse throughout the training process, depicted in Fig. 8(a). Combining the result in the first CQED system, this result shows the general validity of our algorithm for a single-photon generation scheme in the CQED systems with different energy-level structures. The previously defined fidelity increases as the training steps grow, depicted in Fig. 8(b). For the Gaussian-type target single-photon output, the precise value of the fidelity finally reaches 99.45%. For the single-photon generation scheme, we are interested in the output single-photon probability density function $|\phi_{\text{out}}(t)|^2$. For this purpose, the control laser pulse can be a real function during the training process. The fully trained control laser pulse is shown in Fig. 8(c). The result shows that our algorithm can find the optimal control laser pulse for achieving high-fidelity single-photon generation from the 3ES-CQED system as well as the 1ES-CQED system (see Fig. 5), which convincingly proves the advantage of the ML algorithm in flexibility.

We also use our algorithm to find the optimal control laser pulse for the single-photon storage in the 3ES-CQED system described in Sec. II B. We take experimentally available values for the parameters of the system as $\{\kappa_c = 2\pi \times 3$ MHz, $\kappa_l = 0$, $\gamma = 2\pi \times 3.00$ MHz, $g = 2\pi \times 15$ MHz, $\Delta_1 = 72.2$ MHz, $\Delta_2 = 229.1$ MHz, $\Delta_3 = 495.8$ MHz $\}$. The theoretical storage efficiency is estimated as $\eta_{\text{esm}} = \eta_{\text{esc}} 2C / (2C + 1)$ [41] in the parameter range of interest. The system using the values of the parameters g , κ , and γ in [41] can only obtain a low storage efficiency due to physics itself. Here we take g , κ , and γ with the same values as the 1ES-CQED system for single-photon storage to test the performance of our ML algorithm. Note that $\eta_{\text{esc}} = 1$ in our 3ES-CQED system with $\kappa_l = 0$.

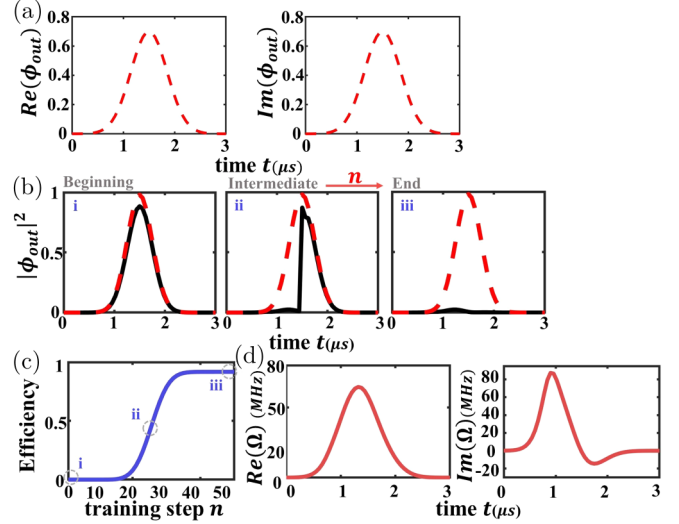


FIG. 9. Single-photon absorption using a 3ES-CQED system with parameters $\kappa_c = 2\pi \times 3$ MHz, $\kappa_l = 0$, $\gamma = 2\pi \times 3.00$ MHz, $g = 2\pi \times 15$ MHz, $\Delta_1 = 72.2$ MHz, $\Delta_2 = 229.1$ MHz, and $\Delta_3 = 495.8$ MHz, and the phase φ of the input photon is $\pi/4$. (a) The real part and the imaginary part of the input single-photon wave function. (b) The input single-photon wave function (dashed red curves) and the leakage (black curves) during the training process. The panels are arranged in the order of training steps from left to right. (c) Storage efficiency increases as the training steps increase. As in Fig. 8, part (b) shows the output wave functions (black curves) at the training steps labeled as (i), (ii), and (iii) in (c). (d) The real part and the imaginary part of the fully trained control laser pulse.

We further prove the validity and robustness of our ML algorithm for storing a single photon with a complex wave function. Without loss of generality, we consider a Gaussian-type complex input single-photon wave function with a phase φ . In this case, the input single-photon pulse ϕ_{in} includes the real part and the imaginary part. We show an example for $\varphi = \pi/4$ in Fig. 9(a). It can be seen from Fig. 9(b) that the corresponding photon leakage $|\phi_{\text{out}}|^2$ approaches zero as the training progresses. The storage efficiency increases during the training and finally reaches 91.78% when the training is finished. The final storage efficiency is slightly less than the theoretical estimated value $\eta_{\text{esm}} = 96.15\%$ [see Fig. 9(c)] due to the detuning of three excited states [41]. Since ϕ_{in} is a complex function, the control laser pulse is also treated as a complex function during the training process. The real part and the imaginary part of the fully trained control laser pulse are shown in Fig. 9(d).

We have also tested our algorithm on single-photon storage where the input wave function phase φ varies between $-\pi/2$ and $\pi/2$, and the corresponding optimal storage efficiency is high, about $92\% \pm 1\%$. We also validate our ML algorithm in the simpler 1ES-CQED system and find that the storage efficiency is about $95\% \pm 0.5\%$ for $\varphi \in (-\pi/2, \pi/2)$, very close to the theoretical estimation of 96.15%. Although the introduction of the phase term significantly increases the complexity of the optimization problem, our ML algorithm is still efficient for finding the optimal control laser pulse for single-photon storage in the 3ES-CQED system as in the 1ES-CQED

system. The results above show that our ML algorithm is effective in a more complex system. This proves its generality and flexibility.

V. DISCUSSION AND CONCLUSION

We have proposed a ML algorithm for on-demand generation and storage of a single photon with an arbitrary wave function by training the control laser pulse applied to a CQED system. By applying an extended Markov assumption and error propagation in training, we achieve nearly unitary generation fidelity and storage efficiency close to the theoretical estimated value even though the single photon has an arbitrary pulse shape and the configuration of the CQED system changes. Our ML algorithm paves the way for building robust quantum networks with a reliable single-photon source and efficient quantum memory.

Identifying a single-photon pulse shape is very useful but is a challenging task. Our ML algorithm may be potentially adapted to identify a single-photon pulse shape via our storage protocol. We can predefine a set of single-photon pulse shapes including the commonly used triangle, square, Gaussian shapes, and many others. Then, our ML algorithm trains a set of control laser pulses for storing these single photons with vanishing leakage or system outputs. It is reasonable to assume that a well-trained control laser pulse can only effectively store a single photon with a certain pulse shape. In this, by finding the shape of the control laser pulse during the storage, we can determine the single-photon pulse shape. For an incoming single-photon pulse, we train its control laser pulse by monitoring the leakage. Then, we identify the single-photon pulse shape from the predefined set with a large success probability according to the control laser pulse shape. This idea may provide a way to use our ML algorithm to identify a single-photon shape, which is unknown but can only take one of the predefined shapes.

ACKNOWLEDGMENTS

K.X. gratefully thanks Prof. Shengjun Wu for his helpful discussion. This work was supported by the National Key R&D Program of China (Grants No. 2019YFA0308700, No. 2017YFA0303703, and No. 2017YFA0303701), the National Natural Science Foundation of China (Grants No. 11874212, No. 11890704, and No. 61671279), and Program for Innovative Talents and Entrepreneurs in Jiangsu (Grant No. JSSCTD202138).

APPENDIX: ALGORITHM SETUP

The hyperparameter choice of the ML algorithm can be adjusted as needed. Here we present the values of the hyperparameters we use in this paper as a reference. The changeable hyperparameters in our ML algorithm include the learning rate η , the number of training steps N , the maximum number of iterations K , and the acceptable minimum error e_{\min} . We set the learning rate η as 0.5 for single-photon generation and a storage scheme in both the 1ES- and the 3ES-CQED system. The numbers of training steps are different for various target wave functions, as shown in Figs. 5(b), 7(b), 8(c), and 9(c). The maximum number of iterations K is kept to 80 in this paper. We also set the acceptable minimum error e_{\min} as the 0.1% of the target value during the training.

The ML algorithm is performed on an Intel Xeon Platinum 8180 CPU with MATLAB 2020. It takes from one-half to one hour to complete the training process with our settings for a specific target wave function in the 1ES-CQED system for both the single-photon generation and the storage scheme. The time consumption varies due to the different choice of the number of training steps N . Note that the complexity of the 3ES-CQED system is higher than that of the 1ES-CQED system. Therefore, it takes 50% longer to finish the full training process for the same target wave function in the 3ES-CQED system as in the 1ES-CQED system.

-
- [1] L. M. Duan, M. D. Lukin, J. I. Cirac, and P. Zoller, *Nature (London)* **414**, 413 (2001).
 - [2] D. Bouwmeester, J.-W. Pan, K. Mattle, M. Eibl, H. Weinfurter, and A. Zeilinger, *Nature (London)* **390**, 575 (1997).
 - [3] E. Knill, R. Laflamme, and G. J. Milburn, *Nature (London)* **409**, 46 (2001).
 - [4] K. Xia, M. R. Vanner, and J. Twamley, *Sci. Rep.* **4**, 5571 (2014).
 - [5] K. Xia and J. Twamley, *Phys. Rev. A* **91**, 042307 (2015).
 - [6] K. Xia, F. Jelezko, and J. Twamley, *Phys. Rev. A* **97**, 052315 (2018).
 - [7] L.-M. Duan and C. Monroe, *Rev. Mod. Phys.* **82**, 1209 (2010).
 - [8] Z.-q. Yin, W. L. Yang, L. Sun, and L. M. Duan, *Phys. Rev. A* **91**, 012333 (2015).
 - [9] X. X. Yuan, J. J. Ma, P. Y. Hou, X. Y. Chang, C. Zu, and L. M. Duan, *Sci. Rep.* **5**, 12452 (2015).
 - [10] H. J. Kimble, *Nature (London)* **453**, 1023 (2008).
 - [11] J. I. Cirac, P. Zoller, H. J. Kimble, and H. Mabuchi, *Phys. Rev. Lett.* **78**, 3221 (1997).
 - [12] M. Brekenfeld, D. Niemietz, J. D. Christesen, and G. Rempe, *Nat. Phys.* **16**, 647 (2020).
 - [13] B. Darquié, M. P. A. Jones, J. Dingjan, J. Beugnon, S. Bergamini, Y. Sortais, G. Messin, A. Browaeys, and P. Grangier, *Science* **309**, 454 (2005).
 - [14] J. Hofmann, M. Krug, N. Ortegel, L. Gérard, M. Weber, W. Rosenfeld, and H. Weinfurter, *Science* **337**, 72 (2012).
 - [15] C.-H. Yuan, L. Q. Chen, Z. Y. Ou, and W. Zhang, *Phys. Rev. A* **83**, 054302 (2011).
 - [16] D. L. Moehring, P. Maunz, S. Olmschenk, K. C. Younge, D. N. Matsukevich, L. M. Duan, and C. Monroe, *Nature (London)* **449**, 68 (2007).
 - [17] S. Gerber, D. Rotter, M. Hennrich, R. Blatt, F. Rohde, C. Schuck, M. Almdross, R. Gehr, F. Dubin, and J. Eschner, *New J. Phys.* **11**, 013032 (2009).
 - [18] B. Lounis and W. E. Moerner, *Nature (London)* **407**, 491 (2000).
 - [19] C. Brunel, B. Lounis, P. Tamarat, and M. Orrit, *Phys. Rev. Lett.* **83**, 2722 (1999).
 - [20] C. Santori, M. Pelton, G. Solomon, Y. Dale, and Y. Yamamoto, *Phys. Rev. Lett.* **86**, 1502 (2001).

- [21] R. B. Patel, A. J. Bennett, I. Farrer, C. A. Nicoll, D. A. Ritchie, and A. J. Shields, *Nat. Photon.* **4**, 632 (2010).
- [22] Y.-M. He, H. Wang, C. Wang, M. C. Chen, X. Ding, J. Qin, Z. C. Duan, S. Chen, J. P. Li, R.-Z. Liu, C. Schneider, M. Atatüre, S. Höfling, C.-Y. Lu, and J.-W. Pan, *Nat. Phys.* **15**, 941 (2019).
- [23] H. Wang, Y.-M. He, T. H. Chung, H. Hu, Y. Yu, S. Chen, X. Ding, M. C. Chen, J. Qin, X. Yang, R.-Z. Liu, Z. C. Duan, J. P. Li, S. Gerhardt, K. Winkler, J. Jurkat, L.-J. Wang, N. Gregersen, Y.-H. Huo, Q. Dai *et al.*, *Nat. Photon.* **13**, 770 (2019).
- [24] R. Brouri, A. Beveratos, J.-P. Poizat, and P. Grangier, *Opt. Lett.* **25**, 1294 (2000).
- [25] H. Bernien, L. Childress, L. Robledo, M. Markham, D. Twitchen, and R. Hanson, *Phys. Rev. Lett.* **108**, 043604 (2012).
- [26] A. Kuhn, M. Hennrich, T. Bondo, and G. Rempe, *Appl. Phys. B* **69**, 373 (1999).
- [27] J. Dilley, P. Nisbet-Jones, B. W. Shore, and A. Kuhn, *Phys. Rev. A* **85**, 023834 (2012).
- [28] S. Y. Chen, L. Q. Chen, Z. Y. Ou, and W. Hang, *Opt. Express* **25**, 031827 (2017).
- [29] L. Q. Chen, G.-W. Zhang, C.-I. Bian, C.-H. Yuan, Z. Y. Ou, and W. Zhang, *Phys. Rev. Lett.* **105**, 133603 (2010).
- [30] A. H. Kiilerich and K. Mølmer, *Phys. Rev. Lett.* **123**, 123604 (2019).
- [31] B. Srivathsan, G. K. Gulati, A. Cere, B. Chng, and C. Kurtsiefer, *Phys. Rev. Lett.* **113**, 163601 (2014).
- [32] S. Zhou, S. Zhang, C. Liu, J. F. Chen, J. Wen, M. M. T. Loy, G. K. L. Wong, and S. Du, *Opt. Express* **20**, 24124 (2012).
- [33] H. P. Specht, C. Nölleke, A. Reiserer, M. Uphoff, E. Figueroa, S. Ritter, and G. Rempe, *Nature (London)* **473**, 190 (2011).
- [34] H. Zhang, X.-M. Jin, J. Yang, H.-N. Dai, S.-J. Yang, T.-M. Zhao, J. Rui, Y. He, X. Jiang, F. Yang, G.-S. Pan, Z.-S. Yuan, Y. Deng, Z.-B. Chen, X.-H. Bao, S. Chen, B. Zhao, and J.-W. Pan, *Nat. Photon.* **5**, 628 (2011).
- [35] M. D. Eisaman, A. André, F. Massou, M. Fleischhauer, A. S. Zibrov, and M. D. Lukin, *Nature (London)* **438**, 837 (2005).
- [36] Z.-Q. Zhou, W.-B. Lin, M. Yang, C.-F. Li, and G.-C. Guo, *Phys. Rev. Lett.* **108**, 190505 (2012).
- [37] J. Guo, X. Feng, P. Yang, Z. Yu, L. Q. Chen, C.-H. Yuan, and W. Zhang, *Nat. Commun.* **10**, 148 (2019).
- [38] K. Zhang, J. Guo, L. Q. Chen, C. Yuan, Z. Y. Ou, and W. Zhang, *Phys. Rev. A* **90**, 033823 (2014).
- [39] T. Chanelière, D. N. Matsukevich, S. D. Jenkins, S. Y. Lan, T. A. B. Kennedy, and A. Kuzmich, *Nature (London)* **438**, 833 (2005).
- [40] T. Li, A. Miranowicz, X. Hu, K. Xia, and F. Nori, *Phys. Rev. A* **97**, 062318 (2018).
- [41] O. Morin, M. Körber, S. Langenfeld, and G. Rempe, *Phys. Rev. Lett.* **123**, 133602 (2019).
- [42] W. Yao, R.-B. Liu, and L. J. Sham, *Phys. Rev. Lett.* **95**, 030504 (2005).
- [43] A. V. Gorshkov, A. André, M. D. Lukin, and A. S. Sørensen, *Phys. Rev. A* **76**, 033804 (2007).
- [44] L. Giannelli, T. Schmit, T. Calarco, C. P. Koch, S. Ritter, and G. Morigi, *New J. Phys.* **20**, 105009 (2018).
- [45] J. Biamonte, P. Wittek, N. Pancotti, P. Rebentrost, N. Wiebe, and S. Lloyd, *Nature (London)* **549**, 195 (2017).
- [46] E. Zahedinejad, J. Ghosh, and B. C. Sanders, *Phys. Rev. Appl.* **6**, 054005 (2016).
- [47] Z. Liu, S. Yan, H. Liu, and X. Chen, *Phys. Rev. Lett.* **123**, 183902 (2019).
- [48] J. Gao, L.-F. Qiao, Z.-Q. Jiao, Y.-C. Ma, C.-Q. Hu, R.-J. Ren, A.-L. Yang, H. Tang, M.-H. Yung, and X.-M. Jin, *Phys. Rev. Lett.* **120**, 240501 (2018).
- [49] X.-L. Huang, J. Gao, Z.-Q. Jiao, Z.-Q. Yan, Z.-Y. Zhang, D.-Y. Chen, X. Zhang, L. Ji, and X.-M. Jin, *Sci. Bull.* **65**, 286 (2020).
- [50] F. Buchkremer, R. Dumke, C. Buggle, G. Birkl, and W. Ertmer, *Rev. Sci. Instrum.* **71**, 3306 (2000).
- [51] B. Unks, N. Proite, and D. Yavuz, *Rev. Sci. Instrum.* **78**, 083108 (2007).
- [52] P. Yun, B. Tan, W. Deng, and S. Gu, *Rev. Sci. Instrum.* **82**, 123104 (2011).
- [53] S. Khan, M. P. Kumar, V. Bharti, and V. Natarajan, *Eur. Phys. J. D* **71**, 1 (2017).
- [54] A. Kuhn, in *Engineering the Atom-Photon Interaction: Controlling Fundamental Processes with Photons, Atoms and Solids*, edited by A. Predojević and M. W. Mitchell (Springer International, Cham, 2015), pp. 3–38.
- [55] R. S. Sutton and A. G. Barto, *Reinforcement Learning: An Introduction* (MIT Press, Cambridge, MA, 2018).
- [56] C. J. Geyer, *Stat. Sci.* **7**, 473 (1992).
- [57] F. Rosenblatt, *Psych. Rev.* **65**, 386 (1958).
- [58] L.-M. Duan and H. J. Kimble, *Phys. Rev. Lett.* **92**, 127902 (2004).
- [59] G. Liu, V. Zakharov, T. Collins, P. Gould, and S. A. Malinovskaya, *Phys. Rev. A* **89**, 041803(R) (2014).
- [60] C. Rogers and P. Gould, *Opt. Express* **24**, 2596 (2016).
- [61] P. Oliveira, S. Addis, J. Gay, K. Ertel, M. Galimberti, and I. Musgrave, *Opt. Express* **27**, 6607 (2019).